

# Multiple-Mouse MRI with Multiple Arrays of Receive Coils (MARCs)

M. S. Ramirez<sup>1</sup>, and J. A. Bankson<sup>1</sup>

<sup>1</sup>The Department of Imaging Physics, The University of Texas M. D. Anderson Cancer Center, Houston, TX, United States

## Introduction

A fundamental goal of MRI research is to improve imaging efficiency. Pulse sequence optimization is critical for minimizing patient scan time in a clinical setting or reducing the overall study duration to achieve sufficient statistical power in preclinical small-animal MRI investigations. The use of phased-array coils (1) and parallel imaging strategies (2) improves the efficiency of MRI by enhancing image quality and allowing for accelerated imaging. Additional efficiency improvements are possible for small-animal MRI by simultaneously scanning multiple animals within a single MRI scanner (3). To date, this has involved either imaging several animals within a single RF coil or by dedicating an independent volume resonator to each animal, which maintains SNR while allowing imaging parameters to be prescribed to simultaneously encode all animals, thus reducing scan time per animal (3,4). The purpose of this work was to investigate the efficacy of a combination of phased-array and multiple-animal MRI technologies to enhance the imaging efficiency and flexibility of small-animal MRI. Multiple arrays of receive coils (MARCs) were used to scan two mice simultaneously with various sensitivity encoding (SENSE) (2) acceleration factors.

## Methods & Materials

A pair of two-element surface coil arrays was fabricated along with a dual-mouse imaging sled for use on a four-channel 7.0T Biospec MRI scanner (Bruker Biospin MRI, Billerica, MA) with a 30 cm bore. Coupling between array elements was minimized by adjusting the loop overlap to minimize mutual inductance and by using lattice-style baluns to reduce unwanted cable interactions. The system was further optimized by remotely tuning and matching each coil element by adjusting the voltage across reversed-biased varactor diodes. This was accomplished via an eight-channel variable voltage system that incorporates automatic coil detuning to decouple the array elements from the transmit birdcage resonator. Water-heating and adjustable anesthesia nose cones were incorporated into the mouse sled which can be moved into and out of the magnet bore along a rail system. The two distinct arrays were separated to both minimize coupling and to maintain simplistic field-of-view (FOV) replication (Fig. 1).

In order to develop the sensitivity maps, an axial full-FOV image ( $FOV_{RO} \times FOV_{PE} = 12 \times 3$  cm; matrix =  $512 \times 128$ ) was acquired through the four coils. Although the full-FOV images were  $12 \times 3$  cm, it was known that no signal would be obtained from the space between the two mice. Thus, the full-FOV images were reduced to  $6 \times 3$  cm, effectively treating the mice as if they were adjacent.  $T_1$ -weighted multi-slice multi-echo (MSME) images ( $TE/TR = 11.8/500$  ms; 12 1-mm slices;  $FOV_{RO} = 3$  cm; matrix<sub>RO</sub> = 128) were then acquired with phase-encoding along the left-right direction. Two-fold ( $FOV_{PE} = 3$  cm; matrix<sub>PE</sub> = 128), three-fold ( $FOV_{PE} = 2$  cm; matrix<sub>PE</sub> = 85), and four-fold ( $FOV_{PE} = 1.5$  cm; matrix<sub>PE</sub> = 64) acceleration factors (AF) were used to scan the abdomen of two mice *in vivo* (Fig.1).

## Results & Discussion

Fig. 2 shows a raw sum-of-squares reconstruction from the four coils along with SENSE-reconstructed mouse images for two and three-fold acceleration factors. As expected, the reconstruction yielded image quality that was inversely related to the acceleration factor. The current findings illustrate the feasibility of using MARCs to dramatically improve the efficiency, flexibility, and reduce the cost of small-animal MRI. Limitations on image quality, SNR, throughput, and the ultimate achievable acceleration factor will be based on principles of parallel imaging, array geometry, and the acquisition protocols employed.

Fig. 1. Illustration of array geometries and prescribed FOVs.

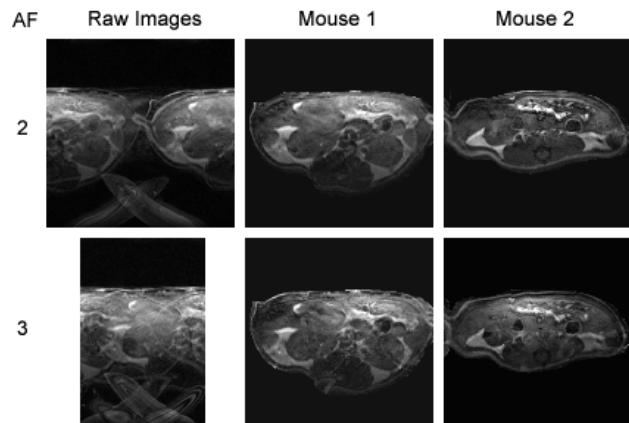
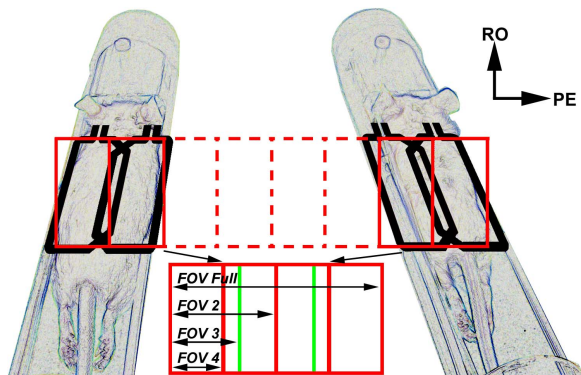


Fig. 2. Raw and reconstructed images for two and three-fold accelerations. Note that the heating water beds were masked out of the images.

## References

- [1] Roemer PB, et al. *Magn Reson Med* 16: 192-225, 1990. [2] Pruessmann KP, et al. *Magn Reson Med* 42: 952-962, 1999. [3] Bock NA, et al. *Magn Reson Med* 49: 158-167, 2003. [4] Ramirez MS, Bankson JA. *J Magn Reson Imag* 26: 1162-1166, 2007.